

# Design, Calibration and Validation of a Novel 3D Printed Instrumented Spatial Linkage that Measures Changes in the Rotational Axes of the Tibiofemoral Joint

**Daniel P. Bonny**

Biomedical Engineering Graduate Group,  
University of California, Davis,  
One Shields Avenue,  
Davis, CA 95616

**M. L. Hull<sup>1</sup>**

Biomedical Engineering Graduate Group,  
University of California, Davis,  
One Shields Avenue,  
Davis, CA 95616;  
Department of Mechanical Engineering,  
University of California,  
Davis One Shields Avenue,  
Davis, CA 95616;  
Department of Biomedical Engineering,  
University of California, Davis,  
One Shields Avenue,  
Davis, CA 95616  
e-mail: mlhull@ucdavis.edu

**S. M. Howell**

Biomedical Engineering Graduate Group,  
University of California,  
Davis, One Shields Avenue,  
Davis, CA 95616;  
Department of Mechanical Engineering,  
University of California, Davis,  
One Shields Avenue,  
Davis, CA 95616

*An accurate axis-finding technique is required to measure any changes from normal caused by total knee arthroplasty in the flexion–extension (F–E) and longitudinal rotation (LR) axes of the tibiofemoral joint. In a previous paper, we computationally determined how best to design and use an instrumented spatial linkage (ISL) to locate the F–E and LR axes such that rotational and translational errors were minimized. However, the ISL was not built and consequently was not calibrated; thus the errors in locating these axes were not quantified on an actual ISL. Moreover, previous methods to calibrate an ISL used calibration devices with accuracies that were either undocumented or insufficient for the device to serve as a gold-standard. Accordingly, the objectives were to (1) construct an ISL using the previously established guidelines, (2) calibrate the ISL using an improved method, and (3) quantify the error in measuring changes in the F–E and LR axes. A 3D printed ISL was constructed and calibrated using a coordinate measuring machine, which served as a gold standard. Validation was performed using a fixture that represented the tibiofemoral joint with an adjustable F–E axis and the errors in measuring changes to the positions and orientations of the F–E and LR axes were quantified. The resulting root mean squared errors (RMSEs) of the calibration residuals using the new calibration method were 0.24, 0.33, and 0.15 mm for the anterior–posterior, medial–lateral, and proximal–distal positions, respectively, and 0.11, 0.10, and 0.09 deg for varus–valgus, flexion–extension, and internal–external orientations, respectively. All RMSEs were below 0.29% of the respective full-scale range. When measuring changes to the F–E or LR axes, each orientation error was below 0.5 deg; when measuring changes in the F–E axis, each position error was below 1.0 mm. The largest position RMSE was when measuring a medial–lateral change in the LR axis (1.2 mm). Despite the large size of the ISL, these calibration residuals were better than those for previously published ISLs, particularly when measuring orientations, indicating that using a more accurate gold standard was beneficial in limiting the calibration residuals. The validation method demonstrated that this ISL is capable of accurately measuring clinically important changes (i.e. 1 mm and 1 deg) in the F–E and LR axes. [DOI: 10.1115/1.4025528]*

## 1 Introduction

The two kinematic axes of the tibiofemoral joint, the flexion–extension (F–E) axis in the femur about which the tibia flexes and extends and the longitudinal rotation (LR) axis in the tibia about which the tibia internally and externally rotates, are parallel and perpendicular, respectively, to the joint line [1] and are unrelated to the anatomic landmarks often used to align prostheses during conventional total knee arthroplasty (TKA) [1,2]. As a result, mechanically-aligned TKA changes the position and orientation of the joint line; thus changing the position and orientation of the F–E and LR axes and consequently the kinematics of the knee. However, the extent to which TKA changes these axes is unknown. An accurate axis-finding technique is required to measure any changes in the F–E and LR axes.

A device that can measure the locations of these axes and thus any changes is an instrumented spatial linkage (ISL), a series of six instrumented revolute joints that can measure the six degrees of freedom of motion (DOF) between two rigid bodies without constraining motion. Previously, we computationally determined how best to design and use an ISL such that rotational and translational errors in locating the F–E and LR axes were minimized [3]. However, this ISL was not constructed and therefore its ability to measure changes in the axes was not validated; computational analysis did not include all sources of error that could be present in an actual ISL, such as compliance of the ISL links, calibration error, and play in the revolute joints.

With one exception, ISLs were previously calibrated using devices that either had no documented accuracy or could not quantify accuracy in every degree of freedom. One ISL was calibrated in a fixture that placed the ISL in various positions that corresponded to knee motion [4]; however, the accuracy of the device was not documented. Three other ISLs were calibrated using precision plates containing dowels of various sizes, shapes, and positions [5–7]; in one case, the accuracy of the calibration device was not documented [5], and in the others the fixture did not

<sup>1</sup>Corresponding author.

Contributed by the Bioengineering Division of ASME for publication in the JOURNAL OF BIOMECHANICAL ENGINEERING. Manuscript received March 28, 2013; final manuscript received September 4, 2013; accepted manuscript posted September 26, 2013; published online November 26, 2013. Assoc. Editor: Sean S. Kohles.

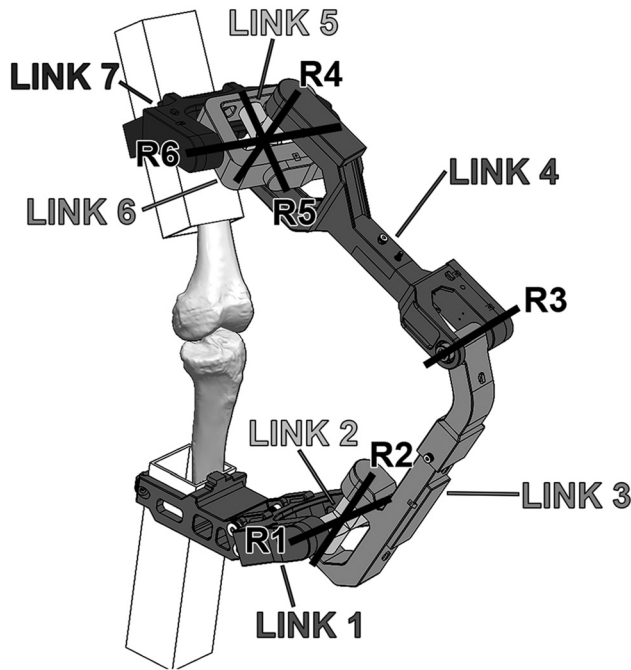


**Fig. 1** An illustration of the ISL attached to a tibiofemoral joint. The six revolute joints are indicated by the black lines and are labeled R1 through R6. Each link is labeled and shaded for clarity.

constrain all degrees of freedom [6,7], and thus accuracy in all degrees of freedom could not be defined. Nordquist and Hull developed a calibration device with precision micrometer pins that was used to calibrate an ISL to the expected range of motion of an ankle [8,9]; the error of this device was quantified and the device was not sufficiently accurate to serve as a gold standard because the device was not at least ten times better than the desired accuracy of the instrument to be calibrated [10]. A calibration method that connected both ends of the ISL to form a closed-loop was recently demonstrated [11]; however, only the calibration residuals were presented thus the accuracy of the method is unknown. Thus, accurately calibrating an ISL requires the development of a new method using a device that is sufficiently accurate to serve as a gold standard in every degree of freedom.

Accordingly, the first objective was to build the ISL that was previously optimized to minimize the errors in measuring the F–E and LR axes [3]. The second objective was to calibrate the ISL using a device that is sufficiently accurate to serve as a gold standard. The third objective was to validate the ISL by quantifying the errors in measuring changes in position and orientation of the F–E and LR axes.

## 2 Materials and Methods

**2.1 ISL Description.** The ISL (Fig. 1) was designed specifically to locate the two axes of rotation of the tibiofemoral joint and was a standard “elbow-type” linkage. An “elbow-type” linkage consists of three intersecting revolute joint axes called the “wrist,” one revolute joint called the “elbow,” and two intersecting revolute joint axes called the “shoulder” [12]; this type of linkage was chosen because it has the largest reachable volume for a given linkage size and can reach all positions and orientations in that volume [12].

The ISL was described using the Denavit–Hartenberg notation [13], a series of coordinate transformation matrixes for each ISL link. The transformation matrix  $[A_i]$ , described the transformation from link  $i$  to link  $i+1$  and was calculated by multiplying, in

**Table 1** The nominal Denavit–Hartenberg parameters describing the ISL. These parameters were previously optimized to minimize the rotational and translational errors when measuring the rotational axes of the tibiofemoral joint [3].

Link $i$	$\alpha_i$ (deg)	$a_i$ (mm)	$s_i$ (mm)	$\theta_i$ offset (deg)
1	90	0	0	150
2	90	0	300	0
3	90	300	0	–150
4	90	0	0	90
5	90	0	0	–90
6	0	0	0	150

order, a variable rotation of  $\theta_i$  about the axis  $z_i$ , a fixed translation of  $s_i$  along the axis  $z_i$ , a fixed translation of  $a_i$  along the axis  $x_{i+1}$ , and a fixed rotation of  $\alpha_i$  about the axis  $x_{i+1}$ . To calculate the global transformation matrix  $[T_{ISL}]$  describing the transformation from the coordinate system of link 1 to the coordinate system of link 7, the transformation matrixes for links 1–6 were consecutively multiplied [14]. Both a slope and an intercept defined each angle  $\theta_i$ ; thus 30 fixed parameters were required to define  $[T_{ISL}]$ .

The Denavit–Hartenberg parameters describing the ISL (Table 1) were chosen because they were previously optimized to minimize the orientation and position errors in locating the rotational axes of the tibiofemoral joint while allowing the knee to flex to a wide range of flexion angles (0 to 130 deg) without colliding with the ISL [3]. The “wrist” of the optimal ISL was attached to the femur while the “shoulder” was attached to the tibia, twist angles were 90 deg for links 1–5 and 0 deg for link 6, and the link offsets and link lengths of links 1 and 4–6 were zero. The links connecting the “elbow” with the “wrist” and “shoulder” were 300 mm long.

The links of the ISL were fabricated using a high-accuracy 3D printer (Eden260V, Objet Geometries Inc., Billerica, MA). The printer has an in-plane print resolution of 0.042 mm, an out-of-plane print resolution of 0.016 mm, and a print accuracy of 0.020–0.200 mm. The print material used to create the links was Objet VeroBlack.

The rotational sensors in the ISL were digital absolute encoders (DS-25-16, Netzer Precision Motion Sensors Ltd, D.N. Misgav, Israel). These encoders were chosen for their high accuracy (maximum absolute error of 0.025 deg) and low mass (4 g). In addition, the rotor assembly was separate from the stator assembly; misalignment of the rotor and stator could be corrected mechanically by adjusting the stator separately from the rotor, thus improving the linearity of each encoder.

The analog output of each encoder was converted to a digital signal in hexadecimal string format within the encoder, thus eliminating the effects of signal noise due to transmission distance. The signals were recorded using custom software developed in LABVIEW (LABVIEW 2011, National Instruments Corporation, Austin, TX) that implemented the Netzer Communication Protocol, a serial input/output command protocol provided by the encoder manufacturer for communication via RS-422.

A two-bearing compression assembly [8] was used for each revolute joint. The screws on each revolute joint simultaneously compressed the bearings against the link assembly and provided an attachment for the rotor of a rotational sensor. The compression assembly was used to eliminate play in the revolute joints and decouple the transducers from any revolute joint loads, thus eliminating the effects of loading on the rotational linearity of each transducer.

**2.2 Calibration.** Two coordinate systems were defined on the ISL using two 10 mm diameter pins with precision flat faces, one each on link 1 and link 7 (Fig. 2). The pin on link 1 was used to define the “base” coordinate system B and the pin on link 7 was

used to define the “end” coordinate system E. The origin of B was the intersection of the axis defining the center of the pin on link 7 and the plane of the face of the pin; the origin of E was similarly defined on link 1. The positive  $\hat{j}_B$  and  $\hat{j}_E$  axes were oriented perpendicular to and directed away from the faces of the respective pins. The  $\hat{i}_B$  and  $\hat{i}_E$  axes were parallel to the sides of links 1 and 7, respectively, and oriented toward the revolute joints of links 1 and 7, respectively. The  $\hat{k}_B$  axis was the cross product of the  $\hat{i}_B$  and  $\hat{j}_B$  axes, and the  $\hat{k}_E$  axis was the cross product of the  $\hat{i}_E$  and  $\hat{j}_E$  axes.

To describe both the relationship between B and the origin of link 1, and the relationship between origin of link 7 and E,  $[T_{1/7}]$  was premultiplied by  $[T_{1/B}]$  describing the transformation from B

to link 1 and post-multiplied by  $[T_{E/7}]$  describing the transformation from link 7 to E. The pre- and post-multiplied transformation matrix defined the transformation from the base coordinate frame B to the end coordinate frame E (Eq. (1))

$$[T_{E/B}] = [T_{E/7}][T_{1/7}][T_{1/B}] \quad (1)$$

Three translations ( $x_B$ ,  $y_B$ , and  $z_B$ ) and three  $Z_\alpha X_\beta Z_\gamma$  Euler angles ( $\alpha_B$ ,  $\beta_B$ , and  $\gamma_B$ ) defined  $[T_{1/B}]$  (Eq. (2))

$$[T_{1/B}] = \begin{bmatrix} \cos \alpha_B \cos \gamma_B - \sin \alpha_B \cos \beta_B \sin \gamma_B & -\cos \alpha_B \sin \gamma_B - \sin \alpha_B \cos \beta_B \cos \gamma_B & \sin \alpha_B \sin \beta_B & x_B \\ \sin \alpha_B \cos \gamma_B + \cos \alpha_B \cos \beta_B \sin \gamma_B & -\sin \alpha_B \sin \gamma_B + \cos \alpha_B \cos \beta_B \cos \gamma_B & \cos \alpha_B \sin \beta_B & y_B \\ \sin \beta_B \sin \gamma_B & \sin \beta_B \cos \gamma_B & \cos \beta_B & z_B \\ 0 & 0 & 0 & 1 \end{bmatrix} \quad (2)$$

Likewise,  $[T_{E/7}]$  was defined by three translations ( $x_E$ ,  $y_E$ , and  $z_E$ ) and three  $Z_\alpha X_\beta Z_\gamma$  Euler angles ( $\alpha_E$ ,  $\beta_E$ , and  $\gamma_E$ ). Including the fixed parameters describing  $[T_{1/B}]$  and  $[T_{E/7}]$ , there were 42 fixed parameters required to define  $[T_{E/B}]$ . However, the parameters  $s_6$ ,  $a_6$ ,  $\alpha_6$ , and the offset of the revolute transducer readout of joint 6 were redundant and thus were defined to be zero because  $[T_{E/7}]$  defined all six degrees of freedom between the coordinate systems of link 7 and E. After excluding those four parameters, 38 fixed parameters remained (Table 2).

The ISL was installed on a calibration fixture developed to hold the ISL in various positions (Fig. 3); the calibration fixture consisted of two axes representing the F–E and LR axes was based on an experimental fixture previously used to simulate a knee [15].

**Table 2 List of the 38 fixed parameters required to define the ISL transformation matrix  $[T_{E/B}]$  and the values of each parameter before and after calibration**

Parameter	Unit	Nominal	Optimized	Difference
$x_B$	mm	54.00	53.81	-0.19
$y_B$	mm	-69.00	-69.85	-0.85
$z_B$	mm	0.00	0.03	0.03
$\alpha_B$	deg	0.00	-0.14	-0.14
$\beta_B$	deg	-90.00	-90.59	-0.59
$\gamma_B$	deg	-60.00	-64.56	-4.56
$\theta_{slope,1}$	deg/deg	1.00	0.99	-0.01
$\theta_{slope,2}$	deg/deg	1.00	0.99	-0.01
$\theta_{slope,3}$	deg/deg	1.00	1.00	0.00
$\theta_{slope,4}$	deg/deg	1.00	1.01	0.01
$\theta_{slope,5}$	deg/deg	1.00	1.00	0.00
$\theta_{slope,6}$	deg/deg	1.00	1.01	0.01
$\theta_{intercept,1}$	deg	150.00	146.93	-3.07
$\theta_{intercept,2}$	deg	0.00	0.21	0.21
$\theta_{intercept,3}$	deg	210.00	208.23	-1.77
$\theta_{intercept,4}$	deg	90.00	89.90	-0.10
$\theta_{intercept,5}$	deg	270.00	270.46	0.46
$\alpha_1$	deg	90.00	90.91	0.91
$\alpha_2$	deg	90.00	89.68	-0.32
$\alpha_3$	deg	90.00	89.20	-0.80
$\alpha_4$	deg	90.00	90.87	0.87
$\alpha_5$	deg	90.00	90.32	0.32
$a_1$	mm	0.00	0.79	0.79
$a_2$	mm	0.00	-1.89	-1.89
$a_3$	mm	300.00	300.78	0.78
$a_4$	mm	0.00	0.34	0.34
$a_5$	mm	0.00	-0.54	-0.54
$d_1$	mm	0.00	-0.02	-0.02
$d_2$	mm	300.00	299.91	-0.09
$d_3$	mm	0.00	0.90	0.90
$d_4$	mm	0.00	0.80	0.80
$d_5$	mm	0.00	-1.41	-1.41
$x_E$	mm	0.00	2.79	2.79
$y_E$	mm	-54.00	-53.73	0.27
$z_E$	mm	94.00	94.82	0.82
$\alpha_E$	deg	90.00	91.91	1.91
$\beta_E$	deg	90.00	90.37	0.37
$\gamma_E$	deg	0.00	-1.34	-1.34

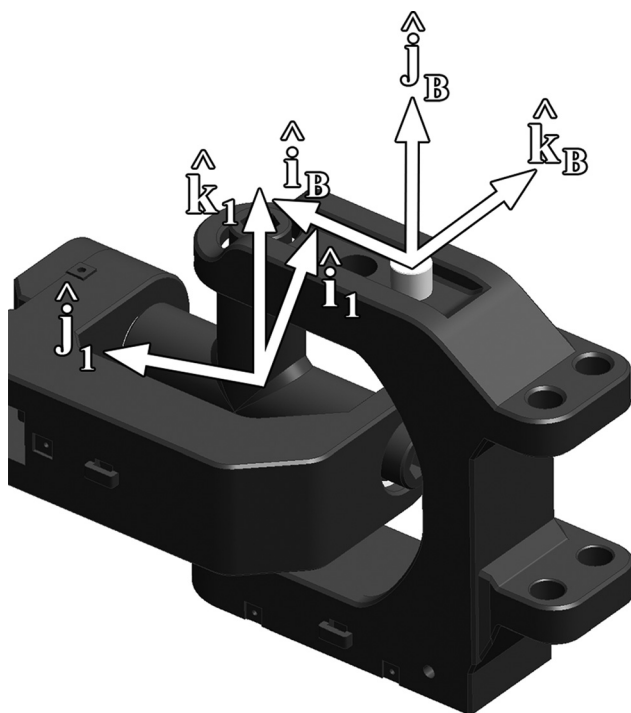


**Fig. 2 A rendering of link 1 of the ISL showing the “base” coordinate system B and the coordinate system of link 1. The origin of B was the intersection of the axis of the pin and the end of the pin. The coordinate system was oriented such that the  $\hat{j}_B$  axis was perpendicular to the face of the pin and the  $\hat{i}_B$  axis was parallel to the side of the link and oriented toward the revolute joint. The coordinate system E was defined identically on link 7 (not shown).**

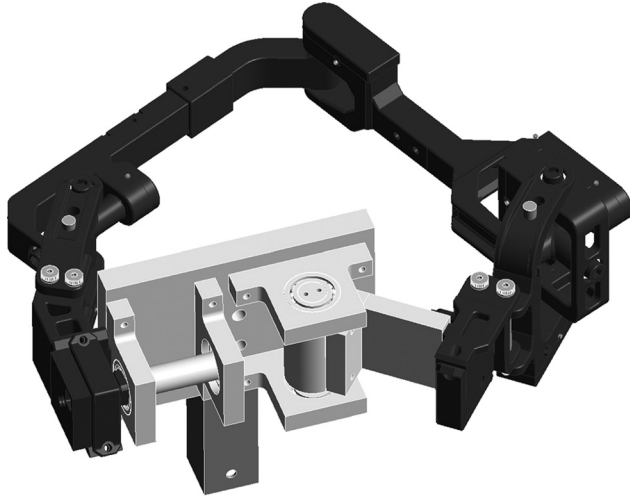


**Fig. 3** A rendering of the calibration fixture (grey) with the ISL (black) attached. The ISL was calibrated on the fixture using the CMM. The calibration fixture consisted of two shafts, pressed into precision bearings, which represented the F–E and LR axes of the tibiofemoral joint.

Link 1 of the ISL was attached to the shaft representing the LR axis, while link 7 of the ISL was attached to the shaft representing the F–E axis. While previous ISLs have been calibrated using a calibration fixture as the gold standard, this calibration fixture was used only to hold the ISL. The ISL was placed in 65 different calibration configurations, representing a range of flexion and I–E rotation angles; the range of flexion was 0 to 120 deg in 10 deg increments, while the range of I–E rotation was –20 to 20 deg in 10 deg increments. At each calibration configuration, the calibration fixture was pinned and the angles of each of the six revolute joints were measured. The transformation matrix  $[T_{E/B}]_k$  was created at each calibration configuration  $k$ .

The coordinate systems B and E were directly measured by a coordinate measuring machine (CMM) at each calibration configuration. The three-linear axis CMM (Model BRT504, Mitutoyo, Aurora, IL) had maximum measurement errors of 2.9–4.9  $\mu\text{m}$  when measuring length and 3.0  $\mu\text{m}$  when measuring diameter; a CMM was chosen to calibrate the ISL because its accuracy is at least ten times better than the desired accuracy of the instrument to be calibrated which satisfies the requirement of a gold standard [10]. For each calibration configuration, 11 points on link 1 and 11 points on link 7 were located by the CMM stylus and were used to locate the coordinate systems B and E (Fig. 4). The coordinate systems B and E measured by the CMM defined the transformation matrix  $[T_{CMM}]_k$ , thus defining the “actual” transformation between the coordinate systems B and E at each calibration configuration  $k$ .

To optimize the 38 fixed parameters describing the transformation from B to E, a cost function was created to calculate the difference, at each calibration configuration  $k$ , between  $[T_{E/B}]_k$  and  $[T_{CMM}]_k$ . The cost function included the residual errors in both position and orientation between the two transformation matrices at every configuration. The residual errors in position and orientation were computed from the transformation matrix between  $[T_{CMM}]_k$  and  $[T_{E/B}]_k$ , defined as  $[T_{CMM/E}]_k$  (Eq. (3))

$$[T_{CMM/E}]_k = [T_{E/B}]_k^{-1} [T_{CMM}]_k \quad (3)$$

The residual errors in position were defined by the 3X1 position partition  $[P_{CMM/E}]$  of the transformation matrix (Eq. (4))

$$[T_{CMM/E}]_k = \begin{bmatrix} R_{CMM/E} & P_{CMM/E} \\ 0 & 1 \end{bmatrix}_k \quad (4)$$



**Fig. 4** A rendering of link 1 of the ISL showing the approximate locations of the eleven surface points measured using the CMM to define the coordinate system B at each calibration position. Four points on the end of the pin formed a plane defining three degrees of freedom necessary to establish a coordinate system. Four points about the pin formed a circle when projected on the end of the pin; thus defining two more degrees of freedom. The three points on the side of the ISL defined the orientation of the coordinate system about the axis of the pin. The coordinate system E was defined using the same procedure; thus 22 points were located for each ISL position.

The residual errors in position were defined as the three position components of  $[P_{CMM/E}]_k$ , defined as  $(P_x)_k$ ,  $(P_y)_k$ , and  $(P_z)_k$ . These three position components defined the anterior–posterior (A–P), medial–lateral (M–L), and proximal–distal (P–D) positions, respectively, at 0 deg flexion. Projection angles were used to compute the residual errors in orientation between  $[T_{CMM}]_k$  and  $[T_{E/B}]_k$  and were defined by the direction cosines from the 3X3 orientation partition  $[R_{CMM/E}]_k$  [14]. The projection angles in the  $x$ -,  $y$ -, and  $z$ -directions were defined as  $(PA_x)_k$ ,  $(PA_y)_k$ , and  $(PA_z)_k$ , respectively (Eqs. (5)–(7))

$$(PA_x)_k = \text{atan} \left( \frac{[R_{CMM/E}(3, 2)]_k}{[R_{CMM/E}(2, 2)]_k} \right) \quad (5)$$

$$(PA_y)_k = \text{atan} \left( \frac{[R_{CMM/E}(1, 3)]_k}{[R_{CMM/E}(3, 3)]_k} \right) \quad (6)$$

$$(PA_z)_k = \text{atan} \left( \frac{[R_{CMM/E}(2, 1)]_k}{[R_{CMM/E}(1, 1)]_k} \right) \quad (7)$$

These three projection angles defined the differences in varus–valgus (V–V), F–E, and internal–external (I–E) orientations, respectively, at 0 deg flexion. The residual errors in position and orientation were then combined into a weighted cost function  $J$  (Eq. (8)), equal to the square of the sum of squared differences in position and orientation at each configuration  $k$ ; the position and orientation components were weighted by  $wt$  defined between 0 and 1

$$J = \sum_{k=1}^n \left[ wt \left\{ (P_x)_k^2 + (P_y)_k^2 + (P_z)_k^2 \right\} + (1 - wt) \left\{ (PA_x)_k^2 + (PA_y)_k^2 + (PA_z)_k^2 \right\} \right]^2 \quad (8)$$

The 38 fixed parameters were calibrated using a nonlinear least-squares curve-fitting algorithm (lsqnonlin) in MATLAB 7.6.0 (The MathWorks, Natick, MA), which is based on an interior-reflective Newton method [16,17]. The algorithm was considered converged after either 100,000 iterations, a change in the cost function of less than 1 E-7, or a change of less than 1 E-7 in all 38 parameters. Of the 65 available calibration configurations, 45 were randomly chosen to calibrate the ISL. The 38 fixed parameters were calibrated 21 times; each time, the same set of 45 calibration

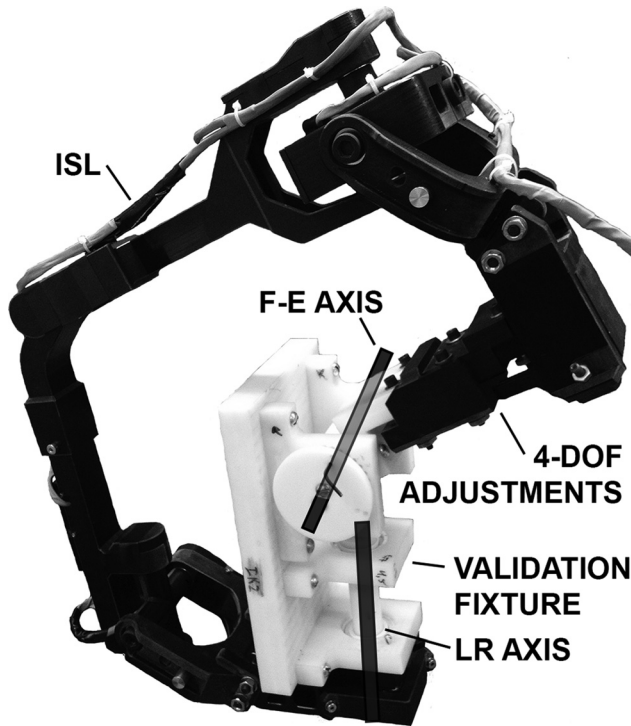


**Fig. 5** A photograph of the validation fixture (grey), shown at approximately 60 deg flexion, with the ISL (black) attached. The validation fixture adjusted the relative positions and orientations of the ISL and the F-E axis in the A-P, P-D, V-V, and I-E degrees of freedom. The validation fixture was similar to the calibration fixture and consisted of two fixed axes that represented the F-E and LR axes and allowed for a flexion range of approximately 0 to 110 deg.

configurations was used but the weighting was adjusted from 0 to 1 in increments of 0.05.

The error of the ISL was quantified for each of the 21 sets of calibrated parameters and the best set was chosen; the error quantities were defined by the bias, precision, and RMSE of each of the six measures of relative position and orientation used to calibrate the ISL ( $P_x$ ,  $P_y$ ,  $P_z$ ,  $PA_x$ ,  $PA_y$ , and  $PA_z$ ). The 20 remaining calibration configurations were used to determine the error of the ISL rather than the 45 used during calibration. The best set of the 38 fixed parameters was the set that minimized the RMSE of each of the measures of relative position and orientation. To better understand the errors in measuring relative position and orientation, each of the six RMSEs were normalized to full-scale range (FSR) across all 65 measured configurations. In addition, to quantify the errors in establishing each coordinate system B and E measured by the CMM, the RMSEs in fitting (1) the four measured points at the end of each pin to a plane, (2) the four measured points around each pin to a circle, and (3) the three points on the side of each link to a line were determined using all 65 calibration positions; all six errors were less than or equal to 0.02 mm.

**2.3 Validation.** A validation fixture was developed to adjust the attachment of the ISL relative to the F-E axis of the fixture and thus quantify the error in measuring a change in the F-E axis (Fig. 5); attachment was modified in the A-P and P-D directions and in the V-V and I-E orientations. The reference surfaces to which the ISL interfaced with the validation fixture were parallel to the F-E axis to ensure that all adjustment directions for the two translations were known. Adjustments to the P-D and A-P positions of the validation fixture ( $\Delta PD$  and  $\Delta AP$ , respectively) were 2.87, 5.08, and 9.74 mm for both positions. Adjustments to the I-E and V-V orientations of the validation fixture,  $\Delta IE$  and  $\Delta VV$ ,

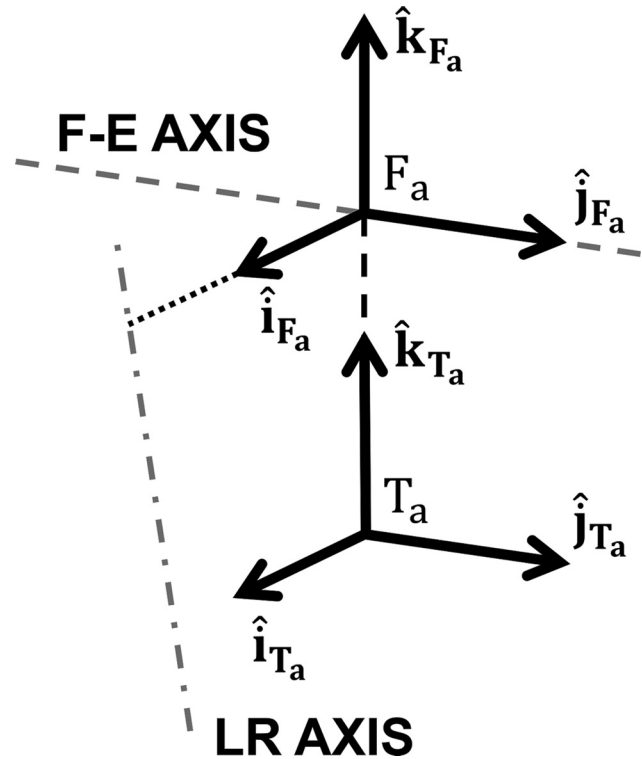


**Fig. 6** A diagram of the anatomic coordinate systems that were defined using the location of the F-E and LR axes of the validation fixture in its reference configuration at 0 deg flexion. The origin of the femoral coordinate system  $F_a$  was on the intersection of the F-E axis and the shortest line connecting the F-E and LR axes at 0 deg flexion. The  $\hat{j}_{F_a}$  axis was coincident with the F-E axis and oriented medially, treating the validation fixture as a right limb. The  $\hat{i}_{F_a}$  axis was oriented anteriorly, coincident with the shortest line connecting the F-E and LR axes. The tibial coordinate system was 20 mm distal to the femoral coordinate system along the  $\hat{k}_{F_a}$  axis.

respectively, were  $-3.0$ ,  $0.0$ , and  $+3.0$  deg for both orientations. Thus, 81 possible configurations of the validation fixture were available. The reference configuration was  $0.0$  deg for  $\Delta IE$ ,  $0.0$  deg for  $\Delta VV$ , and  $2.87$  mm for both  $\Delta PD$  and  $\Delta AP$ .

The ISL was used to locate the axes of the reference configuration of the validation fixture (Fig. 5); the axes were located using an axis-finding algorithm that simultaneously locates the F-E and LR axes [18]. A “sequential discrete” applied motion pattern [3] was used with an I-E rotation range of  $\pm 15$  deg and a total flexion range of 110 deg; both I-E rotation and flexion were applied in 5 deg increments.

Because the “base” and “end” coordinate systems B and E were not aligned with the anatomic directions of a tibiofemoral joint, two additional coordinate systems were created to represent the femoral and tibial anatomic coordinate systems. These two additional coordinate systems, the femoral anatomic coordinate system  $F_a$  and the tibial coordinate system  $T_a$ , were created using the F-E and LR axes of the validation fixture in its reference configuration at 0 deg flexion (Fig. 6). To define the relationship between these two additional coordinate systems,  $[T_{E/B}]$  was premultiplied by  $[T_{F/E}]$ , the transformation between E and  $F_a$ , and post-multiplied by  $[T_{B/T}]$ , the transformation matrix between  $T_a$  and B (Eq. (9))

$$[T_{F/T}] = [T_{F/E}][T_{E/B}][T_{B/T}] \quad (9)$$

Two orientations and two positions were used to describe the measured locations of the F-E and LR axes. The F-E axis was described by two positions (A-P and P-D) and two orientations

**Table 3 ISL errors (i.e. the bias, precision, and RMSE of each measure of relative position and orientation) for the optimal set of fixed parameters computed using the 20 configurations not used to calibrate the ISL. The RMSEs were compared with the full-scale range of each variable across all calibration positions.**

Performance measure	P <sub>x</sub> (mm)	P <sub>y</sub> (mm)	P <sub>z</sub> (mm)	PA <sub>x</sub> (deg)	PA <sub>y</sub> (deg)	PA <sub>z</sub> (deg)
Bias	-0.08	-0.06	-0.03	-0.07	0.05	-0.05
Precision	0.22	0.32	0.14	0.09	0.09	0.08
RMSE	0.24	0.33	0.15	0.11	0.10	0.09
FSR	419.0	113.9	231.4	39.8	119.9	39.7
RMSE (% of FSR)	0.06%	0.29%	0.06%	0.28%	0.08%	0.22%

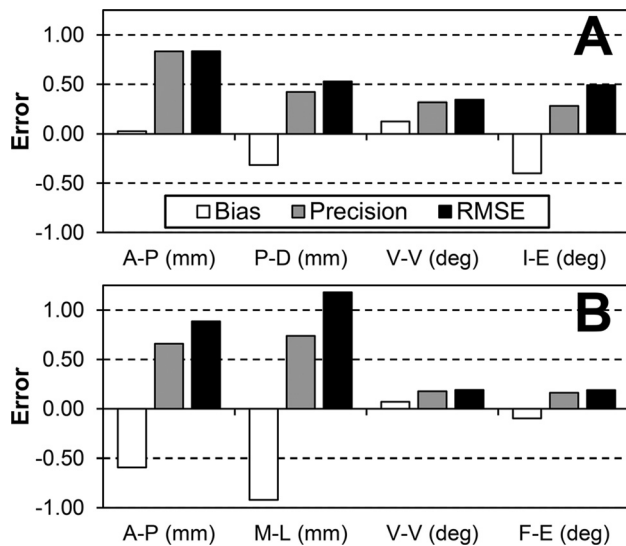


**Fig. 7 The bias, precision, and RMSE in measuring changes to the (a) F–E axis and (b) LR axis. For each position and orientation variable, the errors shown were for the starting flexion angle where the maximum RMSE of each variable occurred.**

(I–E and V–V) describing the position differences and projection angles between the F–E axis and the coordinate system  $F_a$  [3]. Likewise, the LR axis was similarly defined by two positions (A–P and M–L) and two orientations (F–E and V–V) describing the position differences and projection angles between the LR axis and the coordinate system  $T_a$  [3].

The F–E and LR axes were located after each adjustment using the same motion pattern originally used to locate the axes of the validation fixture in its reference configuration. The 110 deg range of flexion was broken into four 60 deg flexion arcs: 20–80, 30–90, 40–100, and 50–110 deg. The starting flexion angles of 0 and 10 deg were not included because the ISL will be used to locate the axes in knees with implanted TKA components that have a different radius from 0 to 10 deg than from 10 deg and beyond, which may change the position and orientation of the F–E axis [2]. The 110 deg flexion limit was chosen to prevent collision of the ISL with the validation fixture.

The actual changes in the F–E axis were determined analytically using the geometric relationships between each part of the validation fixture, which required knowledge of six quantities: the four adjustable quantities ( $\Delta VV$ ,  $\Delta IE$ ,  $\Delta AP$ , and  $\Delta PD$ ) and two additional fixed quantities. In the reference configuration, the two fixed quantities  $L$  and  $D$  defined the perpendicular distances from the F–E axis to the axes about which  $\Delta VV$  and  $\Delta IE$  were adjusted, respectively; these quantities were measured via CMM ( $L = 222.8$  mm,  $D = 7.0$  mm). The actual P–D change in the measured F–E axis (Eq. (10)) was defined as

$$PD_{\text{actual}} = L - (L + \Delta PD) \sec \Delta VV - (D + \Delta AP) \tan \Delta IE \tan \Delta VV \quad (10)$$

Likewise, the actual A–P change in the measured F–E axis (Eq. (11)) was defined as

$$AP_{\text{actual}} = D - (D + \Delta AP) \sec \Delta IE - (L + \Delta PD) \tan \Delta IE \tan \Delta VV \quad (11)$$

Changes in the position of the ISL relative to the F–E axis would not change either measured orientation of the F–E axis; thus the actual V–V and I–E changes in the measured F–E axis were equal to the V–V and I–E changes in the ISL relative to the F–E axis. The actual changes in the LR axis were zero for all adjustments.

The errors in measuring changes in the axes were computed as the differences between the actual and measured changes in the positions and orientations of the F–E and LR axes. These errors were determined for 20 of the available 80 configurations of the validation fixture (81 minus the reference configuration); of these 20 configurations, eight were chosen such that the expected change of only one variable was nonzero and the other 12 were randomly chosen from the remaining 72 configurations. The bias, precision, and RMSE in measuring changes to the axes were calculated for each of the four flexion arcs.

### 3 Results

The optimal set of fixed parameters determined during calibration (Table 2) resulted from a weighting of 0.35. The largest RMSE in measuring relative position (Table 3) was for  $P_y$  (0.33 mm, 0.29% of FSR), which corresponded to the M–L direction, and the smallest was for  $P_z$  (0.15 mm, 0.06% of FSR), which corresponded to the P–D direction. The largest RMSE in measuring relative orientation was for  $PA_x$  (0.11 deg, 0.28% of FSR), which corresponded to V–V orientation and the smallest was for  $PA_z$  (0.09 deg, 0.22% of FSR), which corresponded to I–E orientation.

Regarding the validation, the differences between the actual and measured changes in the F–E and LR axes showed little variation across each of the four starting flexion angles; thus, for each position and orientation variable, the bias, precision, and RMSE were reported only for the starting flexion angle in which the maximum RMSE of each variable occurred (Fig. 7). The RMSEs in measuring changes to the position of the F–E axis were lower than the RMSEs in measuring changes to the position of the LR axis; both position RMSEs for the F–E axis and the A–P RMSE for the LR axis were below 1.00 mm, whereas the M–L RMSE for the LR axis was 1.18 mm. The RMSEs in measuring changes to the orientation of the LR axis were lower than the RMSEs in measuring changes to the orientation of the F–E axis; both orientation RMSEs for the F–E axis were below 0.5 deg and both orientation RMSEs for the LR axis were below 0.25 deg.

### 4 Discussion

Although we previously determined the best design of an ISL to minimize error when locating the F–E and LR axes [3], the ISL was not constructed and thus was neither calibrated nor validated. Previous calibration methods are insufficiently accurate and require the manufacture of calibration devices. Furthermore, no

**Table 4 Improvement in the mean position and orientation errors after calibration over previous ISLs. The ISL was compared only with studies that used a 6-DOF ISL and reported the estimated mean position and orientation errors (i.e. the square root of the normalized sum of the squared residuals [6]).**

Study	Mean position error (mm)	% Improvement	Mean orientation error (deg)	% Improvement
Current study	0.25	NA	0.12	NA
Sommer 1981 [6]	0.20	–	0.50	76%
Lewis 1988 [7]	0.67	63%	0.73	83%
Kirstukas 1992 [4]	0.70	64%	0.40	69%
Nordquist 2007 [8]	1.00	75%	0.59	79%

method has been previously established to evaluate the errors in measuring changes in the F–E and LR axes. Thus the objectives were to (1) construct the ISL that was previously optimized to minimize the errors in measuring the F–E and LR axes [3], (2) calibrate the ISL using a gold standard that was sufficiently accurate, and (3) validate the ISL by quantifying the errors in measuring changes in position and orientation of the F–E and LR axes. The ISL was constructed per the previously described optimized design. The ISL was directly calibrated using a CMM, achieving maximum RMSEs in measuring relative position and orientation of 0.29% FSR and 0.28% FSR, respectively. Validation was performed via a fixture that was developed to apply incremental changes in the F–E axis and was used to quantify the errors in measuring changes in position and orientation of the F–E and LR axes; all orientation RMSEs were below 0.50 deg and only one position RMSE was above 1.00 mm.

There are several advantages and disadvantages in using a CMM to directly calibrate an ISL. One advantage is that the accuracy of the calibration device is known and therefore does not need to be quantified separately from the accuracy of the ISL. Because a gold standard should be an order of magnitude better than the device being calibrated [10], the accuracy of the calibration device must be quantified to be certain of the accuracy of the ISL. Only one previous study reported the accuracy of their calibration device [9]; the absence of documented accuracy for calibration devices could indicate either that a sufficiently accurate gold standard is difficult to manufacture as previously suggested [9], or that quantifying the accuracy of a calibration device is thought to be unimportant. Another advantage is that the calibration method requires only a CMM and a fixture to hold the ISL; previous methods required the manufacture of complicated devices that required additional calibration [4,9,19], thus adding additional sources of error. One disadvantage is that the CMM must be large enough to measure the ISL in all necessary configurations, potentially either limiting the size of the ISL or requiring an unreasonably large CMM. In addition, the ISL must be constructed with measurable features sufficient to define coordinate systems on links 1 and 7. Finally, the calibration method can be time-intensive; approximately 10 min were required to measure all 22 points at each configuration.

The errors after calibration for this ISL were generally better than ISLs calibrated with other methods and were small considering the size of the ISL. Using the square root of the normalized sum of the squared residuals [4,6] to describe the mean position and orientation errors, this ISL had mean position and orientation errors of 0.25 mm and 0.12 deg, respectively. Compared with previous ISLs (Table 4), this ISL improved on the mean orientation error by between 69 and 83%. Except for one ISL which had a lower position error, this ISL improved on the mean position error by between 63 and 75%. The ISL in this study had link lengths that were three times larger than the ISL that had a lower mean position error but higher mean orientation error [6]; thus the design guideline that larger link lengths scale the position errors but not the orientation errors of an ISL [20] is supported by this study. In addition, because this ISL was larger than previous ISLs and thus had larger full-scale ranges, the position and orientation

RMSEs as a percentage of FSR were quite low; no RMSE was higher than 0.29% FSR.

To better evaluate the success of the calibration method, it would be useful to compare the errors in measuring relative position and orientation for this ISL with the errors of a similar device calibrated using a CMM. There is no direct comparison available because no other ISLs have been calibrated with a CMM; however, a 3DOF calibration device with link lengths of 239 and 102 mm was previously calibrated using a CMM [9]. The RMSE of the magnitude of the position errors for the calibration device was 0.66 mm or 0.66% FSR, whereas the RMSE of the magnitude of the position errors of this ISL was 0.43 mm or 0.09% FSR. Thus, the position RMSE was better despite the much larger size of this ISL compared to the calibration device and despite having six revolute joints rather than three. The orientation errors were not comparable because the orientation errors of the calibration device were described using direction angles, while the orientation errors of this ISL were described using projection angles.

Because this ISL will be used to measure changes in the F–E and LR axes after TKA, the errors in measuring these changes must be small so that a clinically important change in either axis can be detected. Because surgical errors less than 1 mm and 1 deg are not reliably attained in the operating room during TKA [21–23], changes in position and orientation of either axis greater than 1 mm and 1 deg, respectively, can be considered clinically important. The highest RMSE in measuring a change to either the F–E or LR axes was in measuring a change to the LR axis in the M–L direction (1.18 mm); all remaining RMSEs in measuring changes to the axes were smaller than 1 mm and 1 deg, respectively (Fig. 6). Therefore, this ISL can be considered sufficiently accurate to measure a clinically important change in position or orientation of either axis.

The RMSEs in measuring changes to the axes (Fig. 6) were higher than the RMSEs in measuring the positions and orientations of the axes that were indicated by the computational analysis [3]. One possible explanation is that the computational analysis only simulated encoder error whereas the actual ISL had more potential sources of error, including error in the Denavit–Hartenberg parameters and deflection of the ISL links. In addition, the validation fixture required disassembly and reassembly between each of the 20 validation combinations. Although the validation fixture had precision reference surfaces to facilitate repeatable assembly, the actual changes to the axes were determined geometrically and were not measured after each change; unknown differences between the actual and true changes to the validation fixture could partly explain the higher RMSEs.

It should be noted that the ISL was not validated to measure the positions and orientations of the F–E and LR axes because only the changes in these axes from the intact knee following TKA will be measured by this ISL. A separate validation would be required to determine the accuracy in measuring the positions and orientations of either axis.

An important assumption of the axis-finding technique used during validation was that the F–E and LR axes are fixed throughout flexion and I–E rotation [18]. Thus, the results of the validation only apply to measuring changes in F–E and LR axes that are

fixed throughout flexion and I–E rotation. This is a valid assumption for the validation fixture because it was constructed using precision bearings. Although previous studies indicate that the two tibiofemoral axes are fixed [1,24,25], reconstructed knees were not investigated; thus it is unknown whether the assumption of fixed axes is valid following reconstruction. However, validation was performed over a partitioned range of flexion (60 deg); thus the assumption of fixed axes must only be valid for a 60 deg flexion arc to measure a change in the axes with the same accuracy as the validation fixture.

The construction of this ISL was improved over previous ISLs in several areas. Steps were taken to reduce the weight of the ISL because a relatively large ISL was required to locate the rotational axes of the tibiofemoral joint across a wide range of flexion [3]. The ISL was fabricated using a light-weight plastic rather than metal to reduce the weight of the ISL. The sensors in this ISL had a mass of only 4 g each; in a previous ISL, sensors that were comparably accurate had a mass of 250 g [18]. Also, the sensors in this ISL were separate from the revolute joints whereas many previous ISLs used the rotational sensors as the revolute joints [18,20,26–28]. Rotational sensors are generally not designed to be load-bearing and free of play; thus if the sensors are used as the revolute joints, then the weight of the ISL links and rotational sensors in conjunction with any play could inflate the apparent nonlinearity of the sensors, particularly in a large ISL.

One limitation in this study was that the LR axis was not validated to the same extent as the F–E axis because the available space between the ISL and the bearings defining the LR axis was not adequate to adjust the attachment of the ISL relative to the LR axis in multiple degrees of freedom. However, because the F–E axis is the dominant axis of the tibiofemoral joint [1] and therefore has a greater effect on tibiofemoral kinematics than the LR axis, this should not be considered a serious limitation.

In summary, there are several important contributions of this work. The ISL in this study was the first to be calibrated directly via a CMM; using this method, the calibration residuals of the ISL were better than those of other published ISLs despite the larger size. No previous studies have quantified the errors when either measuring a change in or locating the F–E and LR axes; the method described herein quantified the error of the ISL in measuring a change in these axes using a simple geometric prediction of the actual changes in the axes. This study indicates that this ISL is sufficiently accurate to detect clinically important changes in the positions and orientations of the F–E and LR axes of the tibiofemoral joint.

## Acknowledgment

We acknowledge the support of the National Science Foundation, Award No. CBET-1067527.

## References

- Hollister, A. M., Jatana, S., Singh, A. K., Sullivan, W. W., and Lupichuk, A. G., 1993, "The Axes of Rotation of the Knee," *Clin. Orthop. Relat. Res.*, **290**, pp. 259–268.
- Eckhoff, D. G., Bach, J. M., Spitzer, V. M., Reinig, K. D., Bagur, M. M., Baldini, T. H., and Flannery, N. M., 2005, "Three-Dimensional Mechanics, Kinematics, and Morphology of the Knee Viewed in Virtual Reality," *J. Bone Joint Surg. Am.*, **87**(Suppl. 2), pp. 71–80.
- Bonny, D. P., Hull, M. L., and Howell, S. M., 2013, "Optimized Design of an Instrumented Spatial Linkage That Minimizes Errors in Locating the Rotational Axes of the Tibiofemoral Joint: A Computational Analysis," *ASME J. Biomech. Eng.*, **135**(3), p. 031003.
- Kirstukas, S. J., Lewis, J. L., and Erdman, A. G., 1992, "6R Instrumented Spatial Linkages for Anatomical Joint Motion Measurement—Part 2: Calibration," *ASME J. Biomech. Eng.*, **114**(1), pp. 101–110.
- Sholukha, V., Salvia, P., Hilal, I., Feipel, V., Rooze, M., and Jan, S. V. S., 2004, "Calibration and Validation of 6 DOFs Instrumented Spatial Linkage for Biomechanical Applications. A Practical Approach," *Med. Eng. Phys.*, **26**(3), pp. 251–260.
- Sommer, H. J., III, and Miller, N. R., 1981, "A Technique for the Calibration of Instrumented Spatial Linkages Used for Biomechanical Kinematic Measurements," *J. Biomech.*, **14**(2), pp. 91–98.
- Lewis, J. L., Lew, W. D., and Schmidt, J., 1988, "Description and Error Evaluation of an In Vitro Knee Joint Testing System," *ASME J. Biomech. Eng.*, **110**(3), pp. 238–248.
- Nordquist, J., and Hull, M. L., 2007, "Design and Demonstration of a New Instrumented Spatial Linkage for Use in a Dynamic Environment: Application to Measurement of Ankle Rotations During Snowboarding," *ASME J. Biomech. Eng.*, **129**(2), pp. 231–239.
- Nordquist, J. A., and Hull, M. L., 2009, "Design and Evaluation of a New General-Purpose Device for Calibrating Instrumented Spatial Linkages," *ASME J. Biomech. Eng.*, **131**(3), p. 034505.
- Doebelin, E. O., 1975, *Measurement Systems: Application and Design*, McGraw-Hill, New York.
- Gatti, G., and Danieli, G., 2007, "Validation of a Calibration Technique for 6-DOF Instrumented Spatial Linkages," *J. Biomech.*, **40**(7), pp. 1455–1466.
- Paden, B., and Sastry, S., 1988, "Optimal Kinematic Design of 6R Manipulators," *Int. J. Robot. Res.*, **7**(2), pp. 43–61.
- Uicker, J., Denavit, J., and Hartenberg, R. S., 1964, "An Iterative Method for the Displacement Analysis of Spatial Mechanisms," *ASME J. Appl. Mech.*, **31**(2), pp. 309–314.
- Paul, R. P., 1981, *Robot Manipulators: Mathematics, Programming, and Control*, MIT Press, Cambridge, MA.
- Roland, M., Hull, M. L., and Howell, S. M., 2011, "Validation of a New Method for Finding the Rotational Axes of the Knee Using Both Marker-Based Roentgen Stereophotogrammetric Analysis and 3D Video-Based Motion Analysis for Kinematic Measurements," *ASME J. Biomech. Eng.*, **133**(5), p. 051003.
- Coleman, T. F., and Li, Y., 1996, "An Interior Trust Region Approach for Non-linear Minimization Subject to Bounds," *SIAM J. Optim.*, **6**(2), pp. 418–445.
- Coleman, T. F., and Li, Y., 1994, "On the Convergence of Interior-Reflective Newton Methods for Nonlinear Minimization Subject to Bounds," *Math. Program.*, **67**(1), pp. 189–224.
- Gatti, G., 2012, "On the Estimate of the Two Dominant Axes of the Knee Using an Instrumented Spatial Linkage," *J. Appl. Biomech.*, **28**(2), pp. 200–209.
- Van Sint Jan, S., Salvia, P., Hilal, I., Sholukha, V., Rooze, M., and Clapworthy, G., 2002, "Registration of 6-DOFs Electrogoniometry and CT Medical Imaging for 3D Joint Modeling," *J. Biomech.*, **35**(11), pp. 1475–1484.
- Kirstukas, S. J., Lewis, J. L., and Erdman, A. G., 1992, "6R Instrumented Spatial Linkages for Anatomical Joint Motion Measurement—Part 1: Design," *ASME J. Biomech. Eng.*, **114**(1), pp. 92–100.
- Nabeyama, R., Matsuda, S., Miura, H., Mawatari, T., Kawano, T., and Iwamoto, Y., 2004, "The Accuracy of Image-Guided Knee Replacement Based on Computed Tomography," *J. Bone Joint Surg. Br.*, **86**(3), pp. 366–371.
- Mizu-Uchi, H., Matsuda, S., Miura, H., Okazaki, K., Akasaki, Y., and Iwamoto, Y., 2008, "The Evaluation of Post-Operative Alignment in Total Knee Replacement Using a CT-Based Navigation System," *J. Bone Joint Surg. Br.*, **90**(8), pp. 1025–1031.
- Mizu-Uchi, H., Matsuda, S., Miura, H., Higaki, H., Okazaki, K., and Iwamoto, Y., 2009, "Three-Dimensional Analysis of Computed Tomography-Based Navigation System for Total Knee Arthroplasty: The Accuracy of Computed Tomography-Based Navigation System," *J. Arthroplasty*, **24**(7), pp. 1103–1110.
- Churchill, D. L., Incavo, S. J., Johnson, C. C., and Beynon, B. D., 1998, "The Transepicondylar Axis Approximates the Optimal Flexion Axis of the Knee," *Clin. Orthop. Relat. Res.*, **356**, pp. 111–118.
- Coughlin, K. M., Incavo, S. J., Churchill, D. L., and Beynon, B. D., 2003, "Tibial Axis and Patellar Position Relative to the Femoral Epicondylar Axis During Squatting," *J. Arthroplasty*, **18**(8), pp. 1048–1055.
- Kinzel, G. L., Hall, A. S., Jr., and Hillberry, B. M., 1972, "Measurement of the Total Motion Between Two Body Segments—I. Analytical Development," *J. Biomech.*, **5**(1), pp. 93–105.
- Salvia, P., Woestyn, L., David, J. H., Feipel, V., Van, S., Jan, S., Klein, P., and Rooze, M., 2000, "Analysis of Helical Axes, Pivot and Envelope in Active Wrist Circumduction," *Clin. Biomech.*, **15**(2), pp. 103–111.
- Ishii, Y., Terajima, K., Koga, Y., Takahashi, H. E., Bechtold, J. E., and Gustilo, R. B., 1995, "Comparison of Knee Joint Functional Laxity After Total Knee Replacement with Posterior Cruciate-Retaining and Cruciate-Substituting Prostheses," *The Knee*, **2**(4), pp. 195–199.